PHYSICAL REVIEW A **83**, 043837 (2011)

# Vortex solitons of the discrete Ginzburg-Landau equation

C. Mejía-Cortés and J. M. Soto-Crespo
*Instituto de Óptica, C.S.I.C., Serrano 121, 28006 Madrid, Spain*

Rodrigo A. Vicencio and Mario I. Molina
*Departamento de Física, Facultad de Ciencias, Universidad de Chile, Casilla 653, Santiago, Chile and*
*Center for Optics and Photonics, Universidad de Concepción, Casilla 4016, Concepción, Chile*
(Received 4 February 2011; published 29 April 2011)

We have found several families of vortex soliton solutions in two-dimensional discrete dissipative systems governed by the cubic-quintic complex Ginzburg-Landau equation. There are symmetric and asymmetric solutions, and some of them have simultaneously two different topological charges for two different closed loops encircling, i.e., centered at, the singularity. Their regions of existence and stability are determined. Additionally, we have analyzed the relationship between dissipation and stability for a number of solutions, finding that dissipation favors the stability of the vortex soliton solutions.

DOI: 10.1103/PhysRevA.83.043837 PACS number(s): 42.65.Wi, 63.20.Pw, 63.20.Ry, 05.45.Yv

## I. INTRODUCTION

An optical vortex soliton is a self-localized nonlinear wave, characterized for having a point ("singularity") of zero intensity, and with a phase that twists around that point, with a total phase accumulation of $2\pi S$ for a closed circuit around the singularity [1]. The quantity $S$ is an integer number known as the vorticity or topological charge of the solution. Optical vortices can exist in an infinite number of ways, as there is no limit to the topological charge. This kind of wave looks attractive in future applications for encoding and storing information. A spatial vortex soliton is a specific solution for a (2+1)-dimensional nonlinear wave equation [2]. One of the most widely used equations of such a type is the nonlinear Schrödinger equation (NLSE). It describes wave evolution in dispersive and diffractive continuous media with an optical Kerr response, i.e., a refractive index that changes linearly with the light intensity. When the system under consideration has a periodic structure, e.g., a photonic crystal fiber, it is necessary to add a periodic transversal potential to complete the description, in the NLSE. The optical properties of a nonlinear periodic structure can be analyzed in the framework of a set of linearly coupled–mode equations, which in solid-state physics is called the *tight-binding* approximation, so that the description of the system can be understood from a discrete point of view. The study of discrete systems has been a hot topic in recent years, due to both its broad impact in diverse branches of science and its potential for technological applications [3–6]. Nonlinear optical systems allow us to observe several self-localized discrete structures in both spatial and temporal domains.

Unlike conservative systems, self-localized structures in systems far from equilibrium are dynamic solutions that exchange energy with an external source (open systems). These solutions are called dissipative solitons [7]. In Schrödinger models, gain and loss are completely neglected and the dynamic equilibrium is reached by means of a balance between the Kerr effect and dispersion or diffraction. For dissipative systems, there must also exist an additional balance between gain and losses, turning the equilibrium into a many-sided process [8]. The Ginzburg-Landau equation is, somehow, a universal model where dissipative solitons are their most interesting solutions. This model appears in many branches of science, such as, for example, nonlinear optics, Bose-Einstein condensates, chemical reactions, superconductivity, and many others [9].

Nonlinear self-localized structures in optical lattices, usually referred to as discrete solitons, have been predicted and observed for one- and two-dimensional arrays [10,11]. The existence of discrete vortex solitons in conservative systems has been reported in several works [12–14]. For the continuous case, dissipative vortex soliton families have been found to be stable for a wide interval of $S$ values [15,16]. Symmetric stable vortices have also been predicted in continuous dissipative systems with a periodic linear modulation [17]. In this work we deal with discrete vortex solitons in dissipative two-dimensional (2D) lattices governed by a discrete version of the Ginzburg-Landau equation. We have found different families of these self-localized solutions. We studied their stability and found stable vortex families for $S = 3$ (symmetric) and $S = 2$ (asymmetric) topological charges for the same set of equation parameters. In addition, we found another symmetric solution in which two topological charges ($S = 2$ and $S = 6$) coexist. Finally, we show how an increase in dissipation increases the size of the stability regions in parameter space for the same "swirl-vortex" soliton solution analyzed in the recent work of Ref. [18].

This paper is organized as follows. In Sec. II we introduce the model that we use in the rest of the paper. Sections III and IV describe the new families of solutions obtained, and in Sec. V we compare the results of our dissipative model with the conservative cubic case (Schrödinger limit). Finally, Sec. VI summarizes our main results and conclusions.

## II. MODEL

### A. The cubic quintic Ginzburg-Landau equation

Beam propagation in 2D dissipative waveguide lattices can be modeled by the following equation:

$$i\dot{\psi}_{m,n} + \hat{C}\psi_{m,n} + |\psi_{m,n}|^2\psi_{m,n} + \nu|\psi_{m,n}|^4\psi_{m,n} = i\delta\psi_{m,n} + i\varepsilon|\psi_{m,n}|^2\psi_{m,n} + i\mu|\psi_{m,n}|^4\psi_{m,n}. \quad (1)$$

 

Equation (1) represents a physical model for open systems that exchange energy with external sources called the (2 + 1)D discrete complex cubic-quintic Ginzburg-Landau (CQGL) equation, where $\psi_{m,n}$ is the complex field amplitude at the $(m,n)$ lattice site, and $\dot{\psi}_{m,n}$ denotes its first derivative with respect to the propagation coordinate $z$. The set

$$\{m = -M, \ldots, M\} \times \{n = -N, \ldots, N\}$$

defines the array, $2M + 1$ and $2N + 1$ being the number of sites in the horizontal and vertical directions (in all our simulations $M = N = 8$). The tight binding approximation establishes that the fields propagating in each waveguide interact linearly only with nearest-neighbor fields through their evanescent tails. This interaction is described by the discrete diffraction operator

$$\hat{C}\psi_{m,n} = C(\psi_{m+1,n} + \psi_{m-1,n} + \psi_{m,n+1} + \psi_{m,n-1}),$$

where $C$ is a complex parameter. Its real part indicates the strength of the coupling between adjacent sites and its imaginary part denotes the gain or loss originated by this coupling. The nonlinear higher-order Kerr term is represented by $\nu$, while $\varepsilon > 0$ and $\mu < 0$ are the coefficients for cubic gain and quintic losses, respectively. Linear losses are accounted for a negative $\delta$.

In contrast to the conservative discrete nonlinear Schrödinger (DNLS) equation, the optical power, defined as

$$Q(z) = \sum_{m,n=-M,-N}^{M,N} \psi_{m,n}(z)\psi^*_{m,n}(z), \tag{2}$$

is not a conserved quantity in the present model. However, for a self-localized solution, the power and its evolution will be the main quantity that we will monitor in order to identify different families of stationary and stable solutions.

We look for stationary solutions of Eq. (1) of the form $\psi_{m,n}(z) = \phi_{m,n}\exp(i\lambda z)$, where $\phi_{m,n}$ are complex numbers and $\lambda$ is real. We are interested by the fact that the phase of solutions changes azimuthally an integer number ($S$) of $2\pi$ in a closed circuit. In such a case, the self-localized solution is called a discrete vortex soliton [19] with vorticity $S$. By inserting the previous ansatz into model (1) we obtain the following set of $(2M + 1) \times (2N + 1)$ algebraic coupled complex equations:

$$\begin{aligned} &-\lambda\phi_{m,n} + \hat{C}\phi_{m,n} + |\phi_{m,n}|^2\phi_{m,n} + \nu|\phi_{m,n}|^4\phi_{m,n} \\ &\quad = i\delta\phi_{m,n} + i\varepsilon|\phi_{m,n}|^2\phi_{m,n} + i\mu|\phi_{m,n}|^4\phi_{m,n}. \end{aligned} \tag{3}$$

We have solved Eqs. (3) using a multidimensional Newton-Raphson iterative algorithm. The method requires an initial guess, and we have found that usually converges rapidly by starting with a highly localized profile seed that can be constructed by a procedure similar to the one described in [18].

### B. Linear stability analysis

Small perturbations around the stationary solution can grow exponentially, leading to the destruction of the vortex soliton. A linear stability analysis provides us the means for establishing which solutions are stable. Let us introduce a small perturbation $\tilde{\phi}$ to the localized stationary solution

$$\psi_{m,n} = [\phi_{m,n} + \tilde{\phi}_{m,n}(z)]e^{i\lambda z}, \quad \tilde{\phi}_{m,n} \in \mathbb{C}. \tag{4}$$

Then, after replacing Eq. (4) into Eq. (1) and after linearizing with respect to $\tilde{\phi}$, we obtain

$$\begin{aligned} &\dot{\tilde{\phi}}_{m,n} + \hat{C}\tilde{\phi}_{m,n} - i\delta\tilde{\phi}_{m,n} \\ &\quad + [2(1-\varepsilon)|\phi_{m,n}|^2 + 3(\nu-\mu)|\phi_{m,n}|^4 - \lambda]\tilde{\phi}_{m,n} \\ &\quad + [(1-\varepsilon)\phi^2_{m,n} + 2(\nu-\mu)|\phi_{m,n}|^2\phi^2_{m,n}]\tilde{\phi}^*_{m,n} = 0. \end{aligned} \tag{5}$$

The solutions for the above homogeneous linear system can be written as

$$\tilde{\phi}_{m,n}(z) = C^1_{m,n}\exp[\gamma_{m,n}z] + C^2_{m,n}\exp[\gamma^*_{m,n}z], \tag{6}$$

where $C^{1,2}$ are integration constants and $\gamma_{m,n}$ is the discrete spectrum of the eigensystem associated with (5). The solutions are unstable if at least one eigenvalue has a positive real part, that is, if $\max\{\mathrm{Re}(\gamma_{\mathrm{m,n}})\} > 0$. Hereafter, we plot stable (unstable) solutions using solid (dashed) lines.

## III. SYMMETRIC AND ASYMMETRIC SOLUTIONS

Equation (1) has a five-dimensional parameter space, namely, $C,\delta,\varepsilon,\mu,\nu$. In order to look for any stationary solution, we need to first choose a fixed set of values for these parameters and then an initial condition. By starting from a guess with eight peaks surrounding the central site, the first discrete contour of the lattice of around $(m,n) = (0,0)$, with a topological charge $S = 3$ sampled on this path, the iterative algorithm rapidly converges to a stationary structure with the same features as the initial guess. Once we find a stationary solution with the desired properties, we use it as the initial condition to find the corresponding solution for a slightly different set of equation parameters. We usually change just one of them. Therefore, for the dissipative case we construct families of solutions by fixing four parameters and varying the fifth one, usually the cubic gain parameter $\varepsilon$.

Using this procedure, we have constructed the **A** family (displayed as the curve $Q$ vs $\varepsilon$ in Fig. 1). We started from a highly localized solution and we slowly decreased the nonlinear gain, observing that the solution became gradually more and more extended as $\varepsilon$ (and $Q$) decreased. More specifically, the values for $Q$ on this family diminish parabolically, reaching the saddle-node point at $\varepsilon \approx 0.62$, where the curve turns around and a new, unstable family emerges. Similar behavior was reported in Ref. [20] for dissipative bright solitons.

Figure 2 shows the amplitude and phase profiles corresponding to the solution marked with a green dot on the **A** family in Fig. 1. From the amplitude profile, Fig. 2(a), we can see how the stationary solution maintains the eight excited peaks of the initial seed. Besides, we can see some energy in the tails, i.e., on the second discrete contour. On the other hand, the phase profile, Fig. 2(b), shows a topological charge of $S = 3$.

A similar procedure has been followed to construct another family, labeled **B** (see Fig. 1). This family consists of asymmetric stationary solutions characterized for having six peaks located on the corners of an elongated hexagon in the $n$-axis direction of the lattice. This spatial configuration

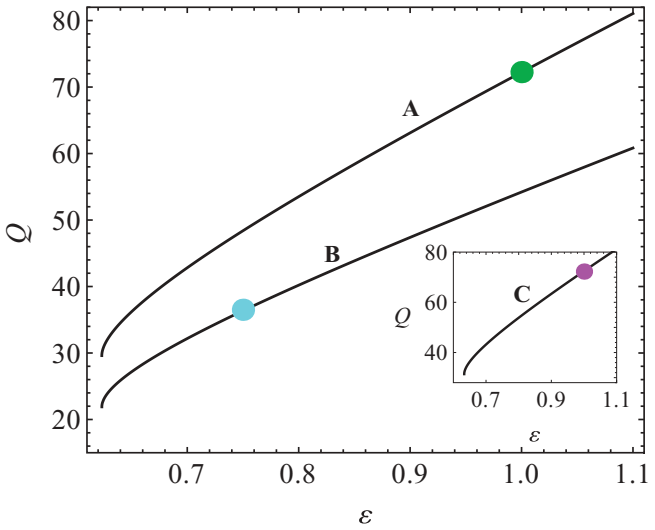


FIG. 1. (Color online) $Q$ vs $\varepsilon$ diagram for families **A** and **B** of discrete dissipative vortex solitons. Inset: $Q$ vs $\varepsilon$ diagram for family **C**. (CQGL equation parameters: $C = 0.8$, $\delta = -0.9$, $\mu = -0.1$, $\nu = 0.1$).

possesses a topological charge of $S = 2$. Typical amplitude and phase profiles for this kind of solution are shown as color maps in Fig. 3. In the conservative case, four-peak structures have been reported to be stable [19] for $S = 1$ and unstable for $S = 2$; on the other hand, for hexagonal lattices, six-peak structures are stable [21] for $S = 2$ and unstable for $S = 1$. In continuous systems, the asymmetric four-peak structure has been found stable for $S = 1$ [22].

The families **A** and **B** of stationary vortex solutions coexist for the same set of parameters of the discrete Ginzburg-Landau equation. Other families of solutions also exist for the same set of parameters. The inset in Fig. 1 shows a different family (family **C**) whose $Q$ vs $\varepsilon$ diagram almost coincides with the **A**-family one, in spite of being a quite different type of solution. We describe these solutions later in Sec. V.

### IV. "Two charges" vortex soliton

We now show one example where two topological charges coexist in the same solution. Let us start with a guess solution consisting of 20 peaks, spatially distributed like a rhombus, and with a topological charge $S = 2$. Using it as the starting point for the Newton-Raphson algorithm, we find a stationary solution that looks like the one shown in Figs. 4(a) and 4(b).

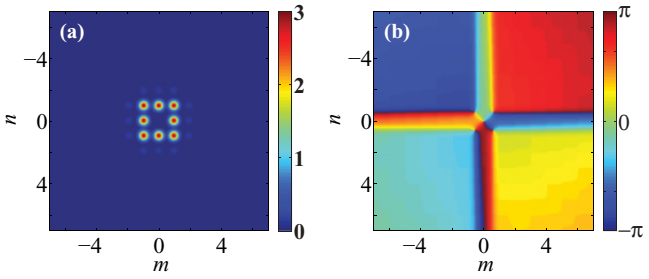


FIG. 2. (Color online) Color map plots for the eight-peak stable vortex solution with $S = 3$, marked with a green dot on the **A** family branch in Fig. 1: (a) amplitude profile and (b) phase profile.

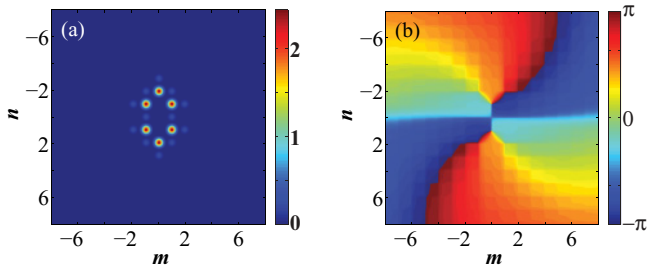


FIG. 3. (Color online) Color map plots for the six-peak stable vortex solution with $S = 2$ marked with a cyan dot on the **B** family branch in Fig. 1: (a) amplitude profile and (b) phase profile.

This solution belongs to the family displayed in Fig. 5, labeled **D**; it was constructed following the same procedure described in the previous section. Unlike the previous families, the **D** family does not reach the saddle-node point via a monotonic decreasing of its power; rather, it passes through a minimum value ($\varepsilon \approx 0.64$), then the power grows, and finally the saddle-node point is reached (see inset of Fig. 5).

The solutions of this family present a very interesting property related to their topological charge. The first square contour $\Gamma_1$, the innermost discrete square trajectory on the plane $(m,n)$ in Fig. 4(b), shows that the vorticity has a value $S = 2$. For the second contour $\Gamma_2$, we observe that the topological charge has changed to $S = 6$. Looking at the remaining contours, we note that the topological charge returns to $S = 2$, so we can talk about a transition of the effective vorticity from $S = 2 \rightarrow S = 6 \rightarrow S = 2$ as we move farther from the center. For this reason, we can say that the stable solutions of this family possess two topological charges.

For the sake of clarity, we plot $\sin(\theta_{m,n})$ vs $\varphi$, the azimuthal angle for the lattice, for the first and second discrete contours. From Fig. 6(a) we can see that the data (green points) are perfectly fitted by the sinusoidal function (gray line) with two periods ($S = 2$) along the first contour, and for the second contour we have six periods ($S = 6$), as shown in Fig. 6(b). This explicitly shows the different topological charges contained in the solution, and it also proves that the discrete vortex is a well-defined structure.

Figure 5 also shows that the **D** family has one large stable region and another small region, magnified in the inset, where

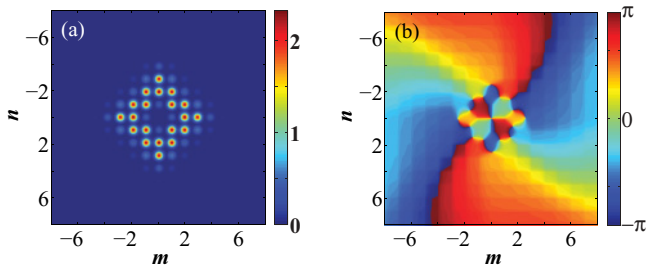


FIG. 4. (Color online) Color map plots for the 20-peak stable two-charge ($S = 2$ and $S = 6$) vortex solution, marked with a green dot on the **D** family in Fig. 5: (a) amplitude profile and (b) phase profile.

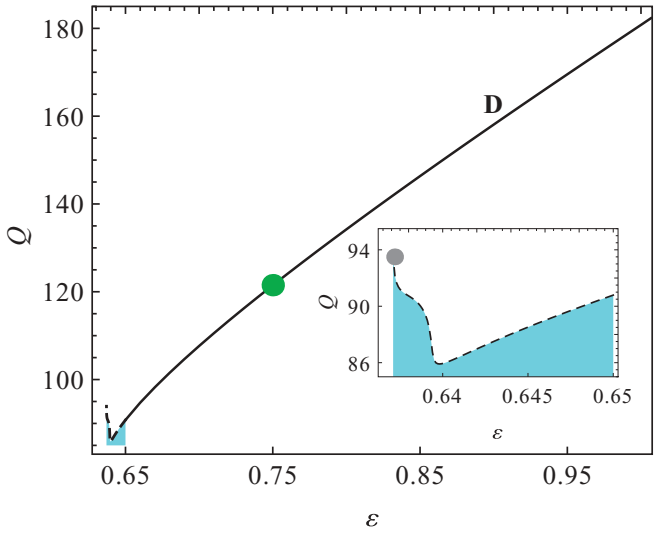


FIG. 5. (Color online) $Q$ vs $\varepsilon$ diagram for "two-charge" ($S = 2$ and $S = 6$) discrete vortex solitons. Continuous and dashed lines correspond to stable and unstable solutions, respectively. The green dot on the **D** family corresponds to the profiles shown in Fig. 4.

the solutions are unstable. These unstable structures decay on propagation to another kind of stable solution having less energy, $S = 2$ vorticity, and a different amplitude profile with only four peaks. In particular, Fig. 7 illustrates how the unstable solution marked with a gray point (the saddle-node point for the **D** family in Fig. 4) decays, by means of a radiative process shown in the inset, to the stable solution marked with a green dot on the **E** family. The amplitude and phase profiles shown in Figs. 8(a) and 8(a) and Figs. 8(c) and 8(d) correspond to the unstable and stable solutions marked with gray and green dots in Fig. 7.

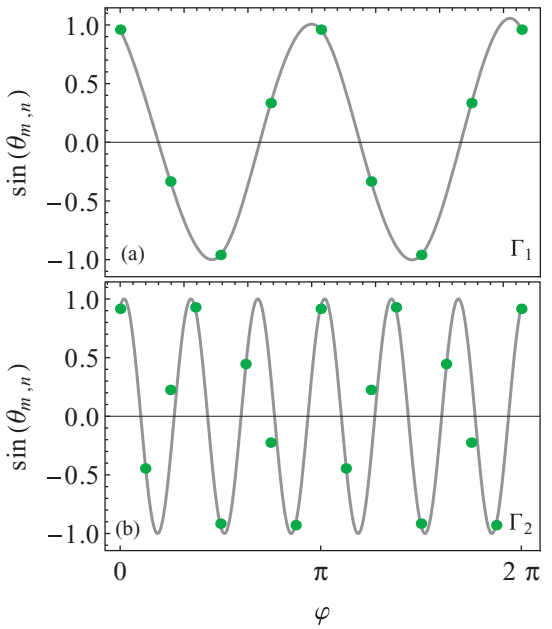


FIG. 6. (Color online) $\sin(\theta_{m,n})$ vs $\varphi$ (azimuthal angle for the lattice) diagram for the first (a) and second (b) discrete contour for the vortex soliton, marked with a green dot on the **D** family in Fig. 5.

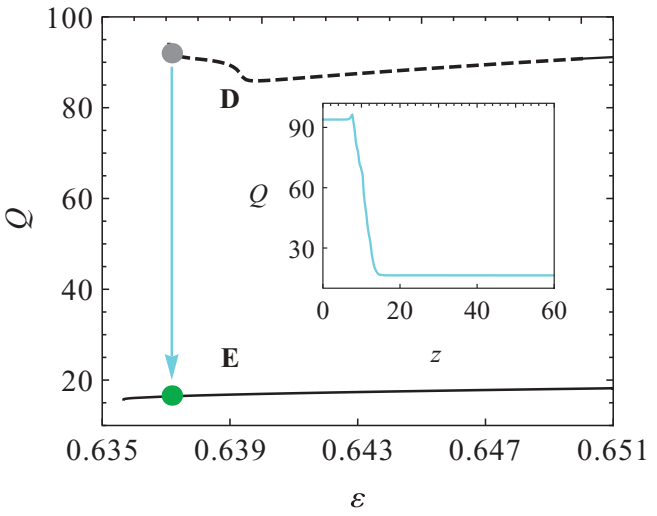


FIG. 7. (Color online) $Q$ vs $\varepsilon$ diagram showing the transition from the unstable solution marked with the gray dot to the stable solution marked with the green dot; the inset shows the power evolution for this transition.

## V. DISSIPATION AND STABILITY

In this section we are interested in analyzing how the stability of the solutions is affected when our model slowly goes to the Schrödinger limit, i.e., when the value of the parameters in the CQGL equation (1) tends to zero: $\{\delta,\epsilon,\mu,\nu\} \to 0$. In particular, we focus on the solution marked with a purple dot on the **C** family in the inset of Fig. 1. This family was found in Ref. [18], after a complicated procedure involving a combination of Newton-Raphson analysis and dynamic evolution. We compute its stability region when the gain, loss,

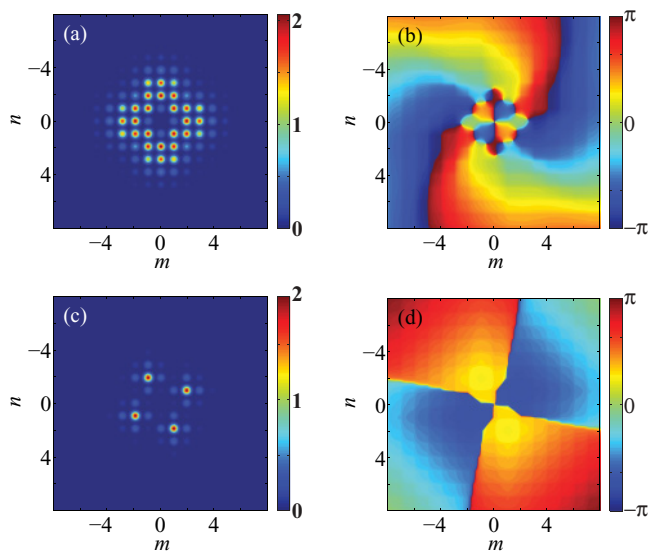


FIG. 8. (Color online) Color map plots for discrete dissipative solitons. (a) Amplitude profile and (b) phase profile for the unstable 20-peak vortex solution localized on the **D** family at the gray dot in Fig. 7. (c) Amplitude profile and (d) phase profile for the four-peak soliton solution localized on the **E** family at the green dot in Fig. 7.

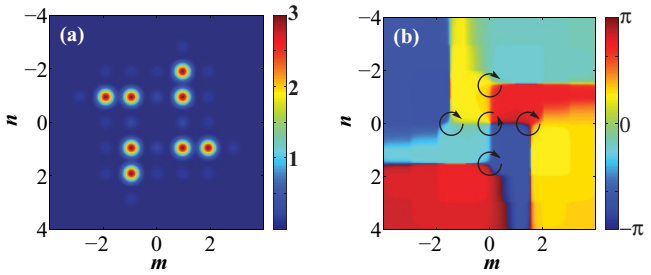


FIG. 9. (Color online) Color map plots for the eight-peak stable two-charge ($S = 1$ and $S = -3$) vortex solution localized on the **C** family at the purple dot in Fig. 1: (a) amplitude profile and (b) phase profile.

and higher order Kerr terms are gradually suppressed in the Ginzburg-Landau model.

These solutions are of the "two-charge" vortex type, with charges $S = 1$ and $S = -3$. Moreover, this type of solutions (the swirl-vortex soliton) can be understood as a bound state of five vortices [23,24]. Indeed, we can identify a vortex with $S = 1$ at the origin (○ symbol), surrounded by four vortex, each with $S = -1$, whose singularities are located at the center of the ↻ symbols in Fig. 9(b). This interpretation agrees with the transition of the effective vorticity from $S = 1 \rightarrow S = -3$, as we move further from the center.

The amplitude and phase profiles for this solution are displayed in Figs. 9(a) and 9(b). Note that it has the same power value as the solution marked with the green dot on the **A** family. (In fact, we plot its corresponding family in the inset because both families have almost identical $Q$ vs $\varepsilon$ diagrams). We can see that both amplitude profiles are very different; even though each one has eight principal excited sites, their spatial distributions are dissimilar. In addition, their

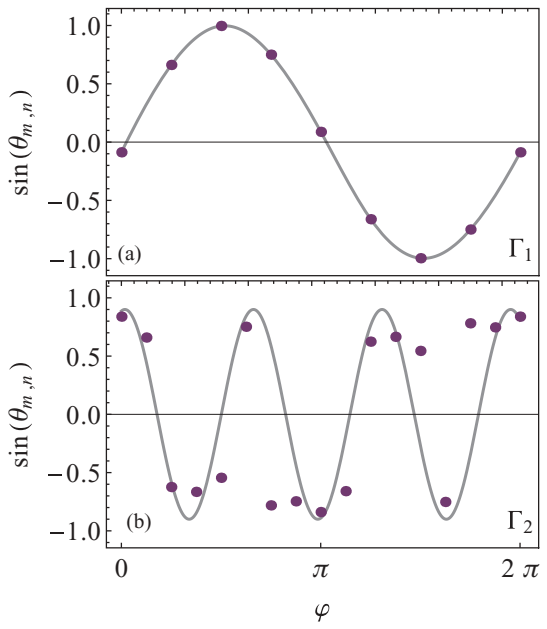


FIG. 10. (Color online) $\sin(\theta_{m,n})$ vs $\varphi$ (azimuthal angle for the lattice) diagram for the first (a) and second (b) discrete contour for the swirl-vortex soliton, marked with a purple dot on the **C** family in Fig. 1.

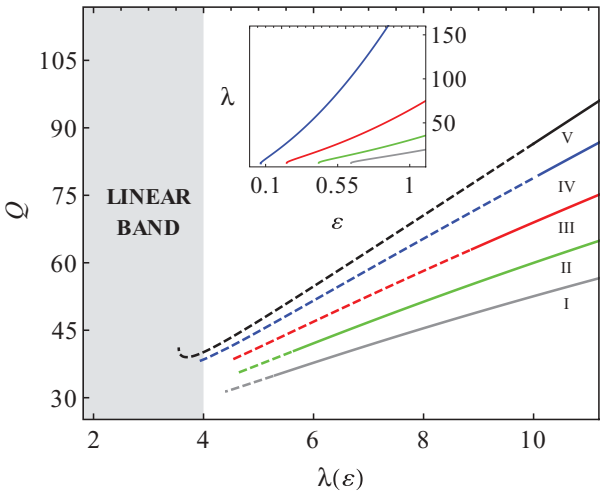


FIG. 11. (Color online) $Q$ vs $\lambda(\varepsilon)$ diagram for several sets of parameters specified in Table I, of two-charge swirl-vortex solitons. Inset shows $\lambda$ vs $\varepsilon$.

phase profiles are completely different. While the solutions on the **A** family have a well-defined unique topological charge $S = 3$, the solutions on the **C** family have two charges ($S = 1$ and $S = -3$) simultaneously, as mentioned before. Again, we plot $\sin(\theta_{m,n})$ vs $\varphi$ for the first ($\Gamma_1$) and the second ($\Gamma_2$) discrete contour. From Fig. 10(a) we can see one period ($S = 1$) for the sinusoidal function (gray line) along the first contour, and for the second contour we have three periods ($S = -3$), as shown in Fig. 10(b). Unlike the conservative cubic case (NLSE), in the dissipative model the propagation constant $\lambda$ is not an arbitrary parameter that can be chosen at will. It is fixed by the rest of the CQGL equation parameters. By changing them, the value of the propagation constant also changes. As in other nonlinear problems [25], we can think of the dissipative terms as determinant to select one of the infinite solutions of the associated conservative problem. With this in mind, we deter the stability regions in terms of the propagation constant so we can compare them with the Schrödinger limit.

For the sake of comparison we construct the $Q$ vs $\lambda$ diagram shown in Fig. 11. Here, we have fixed $\delta$, $\mu$, and $\nu$ parameters and we move only through the $\varepsilon$ parameter (nonlinear gain). In this way, we obtain a solution and its corresponding propagation constant for each value of $\varepsilon$. Then we proceed to vary the rest of the parameters slightly and construct a new curve, taking the solutions of the previous curve as initial conditions in our multidimensional Newton-Raphson scheme. In the inset of Fig. 11 we show the corresponding $\lambda$ vs $\varepsilon$ diagram.

With the previous scheme we can find a large number of curves, but for the sake of clarity, we show only three of them; they are located between the conservative cubic case (black branch) and the **C** curve (gray branch). We can read from Table I the CQGL equation parameters corresponding to the curves displayed in Fig. 11. These five branches belong to the same family composed of vortex solutions with amplitude and phase profiles such as those shown in Fig. 9. We have performed the standard linear stability analysis described in Sec. II

TABLE I. CQGL equation parameters.

| Curve | $\delta$ | $\mu$ | $\nu$ |
|---|---|---|---|
| I | −0.9 | −0.1 | 0.1 |
| II | −0.8 | −0.08 | 0.08 |
| III | −0.4 | −0.03 | 0.03 |
| IV | −0.1 | −0.01 | 0.01 |
| V | 0 | 0 | 0 |

for each of them. As noted at the end of Sec. II, we use continuous (dashed) lines for stable (unstable) solutions

Based on the above, we can clearly establish that if the dissipation is attenuated the stability regions for the soliton solutions are reduced [25]. Indeed, we can see here a large difference between the stability regions for the Schrödinger limit and the **C** branch. The first one only has stable solutions for propagation constant values far away from the linear band; the last one has stable solutions for propagation constant values closer to the linear band.

## VI. SUMMARY AND CONCLUSIONS

In conclusion, we have found discrete vortex solitons (symmetric and asymmetric) with higher-order vorticity in dissipative 2D lattices and studied their stability. In particular, we have shown in detail a solution that contains two topological charges and analyzed the stability of the solutions when dissipation in the system is varied. We observe that the size of the stability region in parameter spaces increases as the dissipation is increased. A comparison with the conservative cubic case is done, showing that dissipation serves to provide stability to otherwise unstable conservative solutions.

## ACKNOWLEDGMENTS

C.M.C. and J.M.S.C. acknowledge support from the Ministerio de Ciencia e Innovación under Contracts No. FIS2006-03376 and No. FIS2009-09895. R.A.V. and M.I.M. acknowledge support from FONDECYT, Grants No. 1080374 and No. 1070897, and from Programa de Financiamiento Basal de CONICYT (FB0824/2008).

[1] C. López-Mariscal and J. C. Gutiérrez-Vega, Opt. Photonics News **20**(5) (2009).
[2] A. S. Desyatnikov, Y. S. Kivshar, and L. Torner, *Progress in Optics* (Elsevier, 2005), Vol. 47, pp. 291–391.
[3] D. K. Campbell, S. Flach, and Y. S. Kivshar, Phys. Today **57**, 43 (2004).
[4] F. Lederer, G. I. Stegeman, D. N. Christodoulides, G. Assanto, M. Segev, and Y. Silberberg, Phys. Rep. **463**, 1 (2008).
[5] S. Flach and A. V. Gorbach, Phys. Rep. **467**, 1 (2008).
[6] R. A. Vicencio, M. I. Molina, and Y. S. Kivshar, Opt. Lett. **28**, 1942 (2003).
[7] *Dissipative Solitons*, edited by N. Akhmediev and A. Ankiewicz, Lecture Notes in Physics (Springer, Berlin, 2005), Vol. 661.
[8] J. M. Soto-Crespo, N. Akhmediev, and G. Town, Opt. Commun. **199**, 283 (2001).
[9] *Dissipative Solitons: From Optics to Biology and Medicine*, edited by N. Akhmediev and A. Ankiewicz, Lecture Notes in Physics (Springer, Berlin, 2008), Vol. 751.
[10] H. S. Eisenberg, Y. Silberberg, R. Morandotti, A. R. Boyd, and J. S. Aitchison, Phys. Rev. Lett. **81**, 3383 (1998).
[11] J. W. Fleischer, M. Segev, N. K. Efremidis, and D. N. Christodoulides, Nature **422**, 147 (2003).
[12] B. A. Malomed and P. G. Kevrekidis, Phys. Rev. E **64**, 026601 (2001).
[13] D. N. Neshev, T. J. Alexander, E. A. Ostrovskaya, Y. S. Kivshar, H. Martin, I. Makasyuk, and Z. Chen, Phys. Rev. Lett. **92**, 123903 (2004).
[14] E. Arévalo, Phys. Rev. Lett. **102**, 224102 (2009).
[15] J. M. Soto-Crespo, N. Akhmediev, C. Mejía-Cortés, and N. Devine, Opt. Express **17**, 4236 (2009).
[16] V. Skarka, N. B. Aleksić, H. Leblond, B. A. Malomed, and D. Mihalache, Phys. Rev. Lett. **105**, 213901 (2010).
[17] H. Leblond, B. A. Malomed, and D. Mihalache, Phys. Rev. A **80**, 033835 (2009).
[18] C. Mejía-Cortés, J. M. Soto-Crespo, M. I. Molina, and R. A. Vicencio, Phys. Rev. A **82**, 063818 (2010).
[19] D. Pelinovsky, P. Kevrekidis, and D. Frantzeskakis, Physica D: Nonlinear Phenom. **212**, 20 (2005).
[20] N. K. Efremidis, D. N. Christodoulides, and K. Hizanidis, Phys. Rev. A **76**, 043839 (2007).
[21] B. Terhalle *et al.*, Phys. Rev. A **79**, 043821 (2009).
[22] T. J. Alexander, A. A. Sukhorukov, and Y. S. Kivshar, Phys. Rev. Lett. **93**, 063901 (2004).
[23] M.-A. García-March, A. Ferrando, M. Zacarés, S. Sahu, and D. E. Ceballos-Herrera, Phys. Rev. A **79**, 053820 (2009).
[24] C. Chong, R. Carretero-González, B. Malomed, and P. Kevrekidis, Physica D: Nonlinear Phenom. **238**, 126 (2009).
[25] J. M. Soto-Crespo, N. N. Akhmediev, B. C. Collings, S. T. Cundiff, K. Bergman, and W. H. Knox, J. Opt. Soc. Am. B **17**, 366 (2000).